

Factors influencing nearshore hypoxia in the southeastern Arabian Sea: A sensor-based study

Abdul Azeez, S^{a,†}, Gireeshkumar, T.R^{a*}, Muraleedharan, K.R^a, Vignesh, E.R^a, Jaleel, A.K.U^a, Arya, K.S^a, Ravikumar Nair, C^a, Ratheesh, R^b.

^aCSIR - National Institute of Oceanography, Regional Centre, Kochi - 682 018, India

^bGeo Sciences Division, Space Applications Centre, ISRO, Ahmedabad, India

*Corresponding author's e-mail: gkumar@nio.org

Phone: +914842390814, Fax: +914842390618

[†]Present address: Applied Research Center for Environment and Marine Studies, Research Institute, King Fahd University of Petroleum & Minerals, Dhahran, Kingdom of Saudi Arabia

Abstract

Seasonal upwelling and the associated incursion of hypoxic waters into the coastal zone is a widely studied topic over different upwelling zones. However, its persistence or variations over short time scales are poorly addressed. The present study, therefore, brings out a first report on hourly variations in the temperature, salinity and dissolved oxygen recorded by an environmental data buoy equipped with sensors, deployed in the nearshore waters of Alappuzha (southeastern Arabian Sea) from April to August 2022. The characteristic feature of the Alappuzha coast is the development of mud banks during the southwest monsoon, providing a tranquil environment suitable for continuous sensor-based measurements when the sea remains turbulent elsewhere. The results showed that despite an advance in the upwelling intensity, there is a significant variation in the oxygen concentration in the study domain on a diurnal scale. In general, the nearshore region was under hypoxia during the first half of the day (00:00 to 12:00 hours), which increased steadily to reach normoxic and supersaturated levels during the rest of the day (12:00 to 24:00 hours). Statistical analysis showed that winds significantly correlate to the coastal environment's subsurface oxygen concentration. During the morning hours, the wind was weak, and the water column remained stratified over the subsurface hypoxic water layer. The situation changed in the afternoon (12:00 hours onwards), as there was a steady increase in the local wind speed (> 5 m/s), which was sustained during the rest of the day. A local wind speed > 5 m/s can disturb the stratification and enhance the mixing process from 12:00 to 24:00 hours. The total kinetic energy of 11.5 J/m^3 is the threshold for this oxygen supersaturation. These findings emphasize the role of wind-induced mixing in alleviating coastal hypoxia, highlighting the need for further biogeochemical and ecological investigations into the impacts of alternating oxic-hypoxic conditions in nearshore waters.

Keywords: Dissolved oxygen, hypoxia, coastal upwelling, autonomous observatory, wind

1. Introduction

Deoxygenation in the coastal environment has captured the interest of oceanographers due to its importance in redox-dependent biogeochemical cycles and its implications on ecological functioning (Fennel & Testa, 2019). Oxygen concentrations affect ocean biogeochemical processes and the survival and distribution of marine organisms (Liu et al., 2020). The oxygen levels in some coastal ecosystems may be below threshold levels, impacting fishery, biodiversity and ecosystem dynamics (Altieri et al., 2017; Diaz, 2001; Grantham et al., 2004; Naqvi et al., 2000). Oxygen concentrations below 2 mg/L can cause direct mortality, impact feeding behaviour, movement, growth, and reproductive processes, and reduce habitat quality for marine species (Vaquer-Sunyer & Duarte, 2008). Oxygen depletion can increase vulnerability to the impacts of fishing. Organisms fleeing from hypoxia aggregate at the edges of low-oxygenated waters or wash ashore and are caught by fishers (Breitbart, 2002). The basin-wide drivers, such as upwelling, can interact with transport processes such as tidal cycle, wind, and rainfall to generate complex patterns of temporal variability in dissolved oxygen (DO) (Booth et al., 2012; Diaz et al., 2009; Walter et al., 2014). The development of hypoxia is closely linked to various environmental factors such as wind, rainfall, and river discharge, as highlighted by studies (Huang et al., 2019; Lu et al., 2018; Wei et al., 2016). In addition to the upwelling, local wind forcing plays a regulating role in the stratification stability (Wang et al., 2022). For example, several studies have found that diurnal wind forcing can regulate temperature/salinity oscillations and mixing (Aristizábal et al., 2016; Bonicelli et al., 2014; Kaplan et al., 2003; Woodson et al., 2007). Frequent strong winds can disrupt stratification and prevent hypoxia formation (Wang et al., 2022).

The southeastern Arabian Sea represents (7 °N – 15 °N and 70 °E – 78 °E) a mini eastern boundary upwelling system during the southwest monsoon season characterised by the upwelling of cold, oxygen-deficient and nutrient-rich waters into the coastal region, significantly enhancing the primary productivity and fishery (Johannessen et al., 1987; Shankar & Shetye, 1997; Smitha et al., 2008; Gopalakrishna et al., 2010; Rao et al., 2010; Jayaram & Kumar, 2018). During upwelling events off the southwest coast of India, key features include the shoaling of the mixed layer towards the coast, southwesterly wind in the offshore, westerly/northwesterly winds nearshore, and the southward flow of the West India Coastal Current (WICC) (Fig. 1b) (Chacko et al., 2012; Mathew et al., 2003). Ekman transport (ET) and surface water divergence are induced by alongshore winds, particularly when they blow parallel to the coast (Fig. 1b), leading to upwelling. Additionally, Ekman pumping, influenced by wind stress curl, contributes to vertical water movement. Notably, alongshore wind stress is recognized as the primary driver of coastal upwelling in the Southeastern Arabian Sea (SEAS) (Shetye et al., 1990).

The Alappuzha mudbank region is situated on the southwest coast of India and is characterised by a highly calm environment with high biological production during the turbulent monsoon season (Fig. 1) (Muraleedaran et al., 2019; Gireeshkumar et al., 2017; Gireeshkumar et al., 2020). This region's abundant fish availability and tranquillity attract fishermen to deploy their platform for fishing activities (Gopinathan & Qasim, 1974; Rao et al., 1984). Alappuzha mud bank is spread over a small area of 20 to 30 km² with a total stretch of 8 km offshore and 4 km alongshore in a semi-circular shape (Balachandran, 2004; Gireeshkumar et al., 2017; Muraleedharan et al., 2018). Studies have attributed the mud bank phenomena that appear along the southwest coast of India during the southwest monsoon to the development of a fluid mud layer (< 2 m) near the bottom (Gireeshkumar et al., 2020). A stable fluid mud layer (from May to September) in the sea bottom effectively dampens and attenuates the energy of the incoming waves, leading to the tranquillity of the mud bank (Mac Pherson and Kurup, 1981; Mathew and Baba, 1995; Muraleedharan et al., 2018; Samiksha et al., 2017). A stable fluid mud layer near the sea bottom is the main causative factor for the formation of mud banks. Once this fluid mud disappears from the region, wave activity dominates. This phenomenon is not permanent throughout the year but is recurrent in many locations (Gireeshkumar et al., 2020).

Many studies reported the variability of salinity, wind, sea surface temperature (SST), DO, coastal hypoxia and nutrient-rich water in the Alappuzha mud bank (Seshappa, 1953; Seshappa & Jayaraman, 1956; Gireeshkumar et al., 2017; Muraleedharan et al., 2017; Mathew et al., 2020; Suneela & Sureshkumar, 2021). The simultaneous occurrence of water column stratification and organic matter decomposition in the bottom water is crucial for establishing and maintaining hypoxic conditions (Diaz, 2001). As a part of the western continental shelf, the mud bank region responds quickly to meteorological changes (wind and rainfall) and synoptic-scale phenomena (upwelling). During high rainfall events, Thottappally Spillway near the Alappuzha mud bank region creates a pathway for spilling excess water from the Pamba basin to the Arabian Sea (Kamranuddin et al., 2021; Modi et al., 2021; Sreejith, 2013). The upwelling intensity and hypoxia along the southwest coast of India can be propagated to very shallow depths (< 3 m) in the mud banks, leading to water column denitrification (Gireeshkumar et al., 2017; Mathew et al., 2019).

Upwelling influences the oxygen concentration of the nearshore environment, which maintains a balance between the degree of deoxygenation of source waters (derived from the shelf edge) and the cumulative oxygen sources and sinks within the system. The sources include oxygen flux in the water column (mainly air-sea gas exchange) and photosynthesis. The sinks comprise various biogeochemical processes such as respiration, nitrification, metal reduction, and sulphate reduction. Hypoxia or anoxia occurs when the sinks exceed the sources for a longer duration, ultimately leading to the development

of dead zones. Upwelling-induced nearshore hypoxia is prevalent along the southwest coast of India, and the drivers behind the development and sustenance of hypoxia are not studied. A better understanding of various factors influencing oxygenation and deoxygenation of nearshore waters is essential for effectively managing and utilising marine resources. We hypothesised that local meteorological factors significantly change the nearshore temperature, salinity and oxygen dynamics, which can substantially impact biogeochemistry and ecosystem functioning, including fishery. In this study, a time-series data set of temperature, salinity and DO was collected at 30-minute intervals by an autonomous observation system at the mudbank region of Alappuzha (Fig. 1). The sensor-derived data sets were correlated with meteorological parameters (wind and rainfall) to understand the local and basin-wide factors influencing oxygen dynamics in the nearshore environment of the mud bank. This can provide critical information on developing and sustaining nearshore hypoxia, largely influencing biogeochemistry and ecological functioning.

2. Data and methods

2.1 Oceanographic and Meteorological Data Collection

Conductivity (derived variable salinity), temperature, and turbidity were measured from 3m to 8m water depth in the Alappuzha mud bank region using a CTD profiler (Seabird 19plus) on 22nd May 2022 (10:14 to 12:24 hours at 3 stations) and 30th July 2022 (between 08:30 and 10:24 hours at 4 stations) (Fig. 1c). The wind speed was also recorded using a handheld digital anemometer (AVM-03) during the CTD measurements. The autonomous observatory (data buoy with moored sensors) was installed at 5 km distance from the shoreline (8 m water depth). It measured the temperature, salinity and DO at 3 m water depth (Fig. 1c). An SBE 37-SM/SMP/SMP-ODO MicroCAT (a real-time transmission sensor) was used to measure high-accuracy conductivity, temperature and DO (optical sensor). Data were collected at 30-minute intervals and transmitted to the shore laboratory. The CTD observation stations 3 and 4 are near the autonomous observatory. An automatic weather station (AWS) was installed at the shoreline and recorded the wind speed and direction at 10-minute intervals. Tide and tidal currents were obtained from global tide FES-AVISO. Offshore wind speed and direction for calculating upwelling/ET were downloaded from the ERA5 database (approximately 25 km from the coast). Daily rainfall data was obtained from the Irrigation Department, Government of Kerala, India. Data of major parameters such as DO, salinity, temperature, local wind speed and tide and derived variables such as freshwater fraction (FF) and ET obtained from this study were used to perform multivariate analyses such as correlogram, two-way ANOVA and principal component analysis (PCA). Correlation coefficients (r^2) whose magnitude are between 0.7 and 1.0, 0.4 and 0.7, and less than 0.3 indicate variables that are high, moderate and low correlations, respectively.

Oxygen saturation levels were calculated using the MatLab runtime terminal for a particular temperature and salinity (Weiss, 1970). The DO above this saturated level is termed supersaturated oxygen. The seawater density is calculated using TEOS-10 (Thermodynamic equation of seawater) and is based on a Gibbs function formulation from which all thermodynamic properties of seawater can be derived in a thermodynamically consistent manner. The wind speed from AWS near the buoy location calculates wind-induced current (Equation 1) (Dean & Dalrymple, 1991; Reid, 1957; Van Dorn, 1953; WES-HL, 1996; Wu, 1969).

$$V = 2.5 \times \sqrt{\frac{0.2 \times \tau_{surface}}{\rho_w}} \ln\left(\frac{11Y_0}{kD_{50}}\right) \quad \text{----- (1)}$$

Where V is the wind-induced current speed of water, $\tau_{surface}$ is the shear stress exerted on the water surface by the wind, ρ_w is the density of the water, 'ln' is the natural algorithm (log to the base e), Y_0 (3 m) is the water depth, k (0.018) is the relative bed roughness (relative to the sediment grain size, D_{50}), and D_{50} (0.0035 mm) is the median grain diameter. The kinetic energy of the wind-induced current and tidal current is calculated using Equation 2

$$KE = \frac{1}{2} \rho_w v V^2 \quad \text{----- (2)}$$

Where v is the volume of the water, and V is the wind-induced current/tidal current. Total kinetic energy is the sum of wind-induced KE and tidal KE. The potential energy (PE) of the seawater is calculated using Equation 3

$$PE = \rho_w v g h \quad \text{----- (3)}$$

Where g is the acceleration due to gravity and h (3 m) is the water depth.

The present study used the Ekman transport as a proxy for upwelling intensity (Johannessen et al., 1987; Shankar & Shetye, 1997; Smitha et al., 2008; Sripoonpan & Saramul, 2021). Since upwelling is a large-scale phenomenon induced by the seasonal wind pattern, wind speed obtained from ERA5 at an offshore location (40 km from the shoreline) within the shelf is used to calculate ET. The ET is derived from the wind stress τ (τ_x zonal and τ_y meridional component).

$$\tau_x = \rho_a C_d \sqrt{W_x^2 + W_y^2} \times W_x, \tau_y = \rho_a C_d \sqrt{W_x^2 + W_y^2} \times W_y \quad \text{----- (4)}$$

$$ET_x = \frac{\tau_y}{f\rho_w} \text{ and } ET_y = \frac{\tau_x}{f\rho_w} \quad \text{----- (5)}$$

Where ρ_a (1.225 kg/m³) is the density of the air, ρ_w is the density of the water, C_d is the dimensionless drag coefficient, and f is the Coriolis force ($2\Omega\sin\theta$, where Ω is the angular velocity of the Earth and

θ is latitude). The total ET is calculated using equation 6 (Cropper et al., 2014; Sripoonpan & Saramul, 2021; Varela et al., 2015)

$$ET = -\sin\left(\varphi - \frac{\pi}{2}\right) ET_x + \cos\left(\varphi - \frac{\pi}{2}\right) ET_y \text{ ----- (6)}$$

Where φ is the coastal orientation angle, and the coastline was approximated by a straight line, making an angle of 24° with the north (Ray et al., 2022; Shetye, 1984). The FF is calculated to understand the freshwater (rainfall and river discharge) content in a coastal region (equation 7) (Seena et al., 2019)

$$FF = \frac{S_0 - S}{S_0} \text{ ----- (7)}$$

Where S_0 is the reference value of salinity (35.5), and S is the salinity obtained from the buoy. According to Seena et al. (2019), the classification of the FF is a freshwater/freshwater plume (FF lies between 0.98–0.86), freshwater plume influenced (0.86–0.49), estuarine plume (0.49–0.15) and estuarine plume influenced (0.15–0.01).

The Brunt-Väisälä frequency (BVF) was calculated to measure the stratification (Equation 8) (Donis et al., 2021; Kokoszka et al., 2023; Seena et al., 2022).

$$BVF = \sqrt{-\frac{g}{\rho_w} \frac{d\rho}{dz}} \text{ ----- (8)}$$

Where g is the acceleration due to gravity, ρ_w is the reference bottom density of the water column, and $(\partial\rho/\partial z)$ represents the vertical gradient of density. A high BVF indicates strong stratification and stable conditions, while a low BVF denotes less stratification and is more susceptible to mixing (Donis et al., 2021; Kokoszka et al., 2023; Seena et al., 2022). The BVF is computed by assessing the density gradients between successive depth intervals measured during the cross-shelf observations. For the time-series buoy measurements, the BVF is determined by comparing the density at the buoy's location with the reference bottom density, typically set at 1022 kg/m^3 and obtained from CTD measurements. This approach allows for a more localized assessment of the buoy's specific water column characteristics, taking into account the reference density from the broader CTD measurements.

3. Results and Discussion

The biogeochemical process of the southwest coast of India is dominated by two seasons: southwest and northeast monsoon (Fig. 1a and b). The semi-annual wind reversal is the major reason for the monsoon cycle. The southwest monsoon season is dominated by upwelling, and the associated water column hypoxia makes the region more complex. The western continental shelf of India hosts one of the world's largest oxygen-deficient zones ($0\text{-}20 \text{ }\mu\text{M}$) during the southwest monsoon season

(upwelling) (Naqvi et al., 2000; 2006). The high freshwater influx (~ 300 cm/yr) into the region leads to strong surface layer stratification (low salinity lens) and prevents the aeration of the water column. The current investigation was conducted in the mud bank region of Alappuzha, situated on the southwest coast of India, where we implemented a comprehensive survey sampling strategy tailored explicitly for mud bank conditions. In the subsequent sections, we delve into the hydrographic variations, DO dynamics, and the statistical analyses conducted in this study.

3.1 Hydrographic variation during May and July

The hydrographic variables indicated a clear water column stratification in the nearshore waters during the first half of the day (Fig. 2). The water column exhibited notable horizontal and vertical fluctuations in temperature (ranging from 24 to 30.5 °C) and salinity (ranging from 26 to 35 PSU). In May (as illustrated in Fig. 2a to e), the observational data about temperature and salinity levels indicated the presence of a distinct low-salinity layer within the surface waters, concurrent with lower temperatures and the emergence of subsurface waters characterized by higher salinity due to upwelling processes. Notably, even during May, the water column exhibited thermal stratification, with a discernible temperature gradient of 3°C. The high temperature in upper waters (surface to 2 m) is due to diurnal warming (Azeez et al., 2021). Similarly, salinity measurements revealed a minimum of 26 Practical Salinity Units (PSU) in surface waters and a maximum of 34.43 PSU in deeper layers, resulting in a net salinity difference of 8.43 PSU spanning the entire water column. The reduction in surface water salinity was attributed to sporadic atmospheric occurrences, primarily rainfall events (Fig. 6b) and associated river discharge through the Thottappally spillway, during this temporal interval (Kamranuddin et al., 2021; Modi et al., 2021; Sreejith, 2013). The density distribution analysis unveiled the presence of two well-defined layers, with density values ranging from 1015 kg/m³ (surface) to 1022 kg/m³ (bottom). These layers were distinguished by lower-density water situated atop higher-density water. By July (Fig. 2f to j), the average salinity across the water column was 34.79 PSU. A gradual temperature decline of ~ 4°C was observed in surface waters from the end of May to the end of July. A thermally stratified layer was identified, with surface water temperatures dropping notably to 26.79 °C and bottom water temperatures to ~24°C. From June onwards, a low salinity lens in the surface waters formed through intense precipitation in the coastal zone was evident, which led to thermohaline stratification at considerably shallow depths.

The high turbidity (exceeding 30 NTU) levels near the sea bottom indicated the mud bank formation in the study region (Fig. 2d and i) (Gireeshkumar et al., 2020, 2017; Muraleedharan et al., 2018). Jyothibabu et al. (2018) investigated the vertical distribution of turbidity and photosynthetically active radiation (PAR) in the mud bank region. Their findings revealed distinctive patterns, indicating

the presence of a significantly turbid, fluid, muddy layer close to the seabed. This turbid layer extended from the coastal area to the outer edges of the mud bank. This high turbid fluid mud layer can significantly dampen the incoming wave energy (Muraleedharan et al., 2018; Gireeshkumar et al., 2020). Turbidity levels are comparatively low at the surface layers, even during the active phase of the mud bank (Fig. 2d and i) (Jyothibabu et al., 2018; Karnan et al., 2017). High turbid waters were noticed during strong winds, such as the passage of cyclones or the onset of southwest monsoon (Muraleedharan et al., 2017). During the hydrographic measurements conducted in the study region, weak winds with speeds consistently below 2 m/s (measured using handheld digital anemometer, AVM-03) were observed in both May and July. This observation underscores the limited influence of local wind-induced mixing on the water column, particularly during the morning hours in this area. Overall, hydrographic observations identified two distinct types of stratification: salinity-driven stratification dominated during May, whereas thermal stratification played a more prominent role in distinguishing water column characteristics in July. Based on BVF, strong stratification was evident during May and July, with high BVF values in May. This finding underscores salinity and temperature's significant role in shaping stratified layers.

3.2 Temperature, salinity, and DO from the automated buoy and its relation to physical and meteorological parameters

A gradual cooling of the nearshore waters was noticed during May end and exhibited significant diurnal variations during June and July. Based on Gupta et al. (2016) and several other references, 26 °C can indicate the incursion of upwelled waters to the nearshore environment. Accordingly, the onset of upwelling (presence of cold and oxygen-deficient waters) in the study domain was evident after the third week of May (Fig. 3c). The salinity, temperature, and DO profiles exhibited significant diurnal variations after the third week of May and, during July, the water temperature decreased further to 22 °C (Fig. 3a to c). During April-May, the water temperature was positively correlated with salinity ($p < 0.001$), while with the progress of upwelling (June-July), it became negatively correlated ($p < 0.001$). The water column experienced alternating hypoxia and normoxia during June-July at approximately 12-hour intervals. We selected three representative days for a closer observation of DO, local wind speed and tidal elevation (25th May, 28th May and 6th June 2022) (Fig. 4a to c), which showed a sharp increase in DO concentration after 12:00 hours associated with an increase in local wind speed. The cross-shelf hydrographic parameters in the first half of the day indicated the water column stratification when relatively weak winds prevailed over the region. These observations indicate that even during a persistent upwelling period, local winds can significantly influence the DO concentrations in the coastal environment on a shorter time scale.

The DO varies significantly under various physical parameters, such as temperature and salinity, which act as primary variables. Since primary physical factors (salinity and temperature) regulate the DO concentrations, we have undertaken a detailed analysis of secondary factors that determine the salinity and temperature of the region. Secondary variables such as wind, rain, and tide play a vital role in changing the primary variables, thereby regulating DO concentrations. Fig. 5 shows the hourly variation of oxygen, temperature, salinity, wind and tide from 23rd May to 9th June 2022. During this period, the study captured the variation of oxygen (0.10-10 mg/L), salinity (29.10 to 34.79 PSU), temperature (24.9 to 29.9 °C), local wind speed (0 to 10 m/s) and rainfall (0 to 62.8 mm) with a maximum tidal range of 0.95 m (mixed semidiurnal-micro tide) (Fig. 5a to e and Fig. 6). The upwelling is observed after the third week of May, showing temperature dropping $< 26^{\circ}\text{C}$ and a maximum salinity of 34.79 PSU (Fig. 5c and d). There are several studies based on the upwelling and rapid upward shifting of 26°C isotherms along the southwest coast of India during the summer monsoon season, accompanied by high saline waters (Banse, 1959; Gopalakrishna et al., 2010; Gupta et al., 2016; Kumar and Anand, 2016; Naqvi et al., 2000; Rao et al., 2008; Shah et al., 2019, 2018, 2015; Sharma, 1978; Smitha et al., 2014, 2008).

From 23rd May to 9th June 2022, the temperature dropped to a minimum of 24.9°C (peak upwelling stages), and the oxygen level reached 0.15 mg/L with an average salinity of 34.50 PSU. The average variation of the parameters from 00:00 to 12:00 hours and 12:00 to 24:00 hours is listed in Table 1. The average temperature and salinity were 26.4°C and 34.10 PSU, respectively (Table 1). Generally, upwelling dominated during the first 12 hours except on 26th May, where the upwelling persisted the whole day. During the southwest monsoon, the mean wind direction over the Indian region is from the southwest, which can vary from place to place in the coastal regions (Philip et al., 2013). In this study, the offshore wind speed responsible for upwelling was > 5 m/s, and the wind direction was mostly westerly and northwesterly (Fig. 7a and b). At the same time, the local wind speed was low (< 2 m/s) (Fig. 7c and d) compared to offshore; this suggests that upwelling and its intensity were controlled by seasonal winds (monsoon). The average DO concentration from 00:00 to 12:00 hours was 2.96 mg/L. The analysis during the first 12 hours showed frequent low wind speed and associated episodic hypoxic events.

Conversely, the water column conditions were reversed during the next 12 hours (12:00 to 24:00 hours). The average DO concentration was 6.7 mg/L with a minimum of approximately 0.10 mg/L and a maximum of 10 mg/L on the 25th and 28th May. A sharp increase in DO (a total variation of 10 mg/L in a day) concentrations after 12:00 hours is observed in Fig. 5a. A minimum salinity of 29.10 PSU was observed on 28th May (afternoon), where the rainfall was 62.8 mm (Fig. 5d and Fig.

6). The influence of high rainfall (15 mm/day on average) and associated river discharge from the Thottappally spillway contributed to the salinity reduction. The local wind speed experienced a notable increase, reaching an average wind speed of 5 m/s. The strong wind may be pivotal in inducing substantial mixing within the water column. The stick plots and rose diagram (Fig. 7a to d) clearly illustrated the prevalence of northerly local winds (westerly and northwesterly winds offshore) over the study region. There were no signs of the typical land-sea breeze patterns during the southwest monsoon. These northerly winds that exceed 5 m/s are sufficient to induce mixing of the water columns. The tide data from FES observed spring tide from 28th May to 31st May, where the tidal range between the highest and lowest tide was comparatively large (0.95 m), causing the tidal force to increase. During the spring tide, the strong tidal force during the flood stage pushes the seawater towards the shore, and the ebb phase spreads the low salinity offshore. The initial 12 hours were dominated by low tide water, and the afternoon shows the high tide's dominance. The micro tides (<2 m) with tidal currents of less than 0.3 m/s cannot break down the water column stratification or enhance oxygen replenishment (Chen et al., 2016; Hetzel et al., 2015). The maximum tidal range observed in the present study during spring tide was 0.95 m; therefore, the impact of the tide was minimal, but it can transport the low salinity in favour of wind-induced mixing. Mixing due to the tidal currents can also cause slight aeration, but the energy produced cannot interrupt the stratification. The strong winds during the second half of the day (Fig. 5b) may break the water column stratification, resulting in well-mixed oxygen-saturated nearshore waters.

3.3 Statistical analysis of the data

The correlogram analysis has been performed to understand the controlling factors influencing the DO dynamics during the monsoon season. The correlation matrix of 7 variables, such as oxygen, salinity, temperature, local wind speed, tide (height and currents), FF and ET, is presented in Fig. 8a. The analysis revealed a significant positive correlation of DO with temperature ($r=0.87$), and salinity exhibited a significant negative correlation ($r=-0.81$). Temperature and oxygen were more sensitive to changes in the degree of upwelling than salinity, as indicated by the magnitude of their fluctuations. Wind speed ($r=0.42$) and tide ($r=0.19$) showed a moderate and low positive correlation with DO, respectively. The correlation between minimum salinity within a particular day and the corresponding rainfall showed a moderate negative correlation ($r=-0.61$). The correlation of FF and ET on oxygen was strongly positive ($r=0.81$) and moderately negative ($r=-0.43$), respectively. The dominance of wind is another factor that modulates the daily mixing process and DO, which was evident from the ANOVA test ($p<0.05$).

PCA was employed to investigate the underlying relationships among various environmental parameters influencing DO levels in coastal waters. PCA revealed two principal components, PC I and PC II, which collectively explained 75.17% of the total variability (Fig. 8b); PC I accounted for 60.67%, and PC II contributed 14.5%. PC I was positively loaded with oxygen, temperature, local wind speed, and FF. At the same time, salinity and ET exhibited negative loadings in PC I, each with a slight angular separation from the component. The nearly 180° angle between these two groups of variables indicated that increasing temperature and FF were associated with high DO levels; in contrast, an increase in salinity and ET were linked to hypoxia. Local wind speed emerged as a significant driver of DO dynamics that induce water column mixing. The influence of tides on DO levels was generally negligible, as evidenced by an angle close to 90° between tides and the other parameters, except during spring tide conditions (it may enhance mixing potential). Overall, the PCA analysis elucidated that the PC I primarily represented the shelf edge upwelling process and the impact of rainfall and river discharge on salinity. A subtle shift in the local wind pattern towards PC2 indicated its role in inducing mixing in nearshore waters and modulating the upwelling process. These findings collectively contribute to a comprehensive understanding of the complex interactions and drivers influencing DO variations in the study area.

In summary, the fluctuations in DO levels were driven by the combined influence of three key parameters: salinity, temperature, and localized wind speed. Specifically, lower salinity in surface waters, resulting from increased rainfall and river discharge (mainly from the Thottappally spillway), played a significant role in stratifying the water column. Additionally, variations in DO levels were linked to the upwelling process, marked by changes in temperature and salinity, as well as the effects of local wind-induced mixing. These combined factors contributed to the modulation of DO levels, transitioning them between hypoxic and saturated/supersaturated states and vice versa.

3.4 Dissolved oxygen dynamics in the nearshore environment

During monsoon, the coastline along the southwest coast of India is generally stratified due to river discharge, diurnal heating and coastal upwelling (Narvekar et al., 2021). Stratification and mixing of coastal waters depend on the conversion between kinetic energy (KE) and potential energy (PE) induced by physical and meteorological factors (Simpson, 1981; Simpson et al., 1990; Wang et al., 2022). Statistical analysis revealed the local wind speed, upwelling, and freshwater content as the major controlling factors influencing the DO dynamics with minimal tide impact. Therefore, we calculated the coastal water's KE (local wind-induced and tide-induced) and PE to understand the dynamics of DO. ET, offshore wind speed, BVF, FF, and tide were also compared against the diurnal variations of DO (Fig. 9). The 100% saturation of oxygen was computed as 6.52 mg/L on average for

the corresponding salinity and temperature (Fig. 9a). The values above 100% saturation are shaded in red in Fig. 9a, termed supersaturated, and below the level can be denoted as oxygen-depleted. The oxygen levels < 2 mg/L indicate hypoxic conditions.

The present study revealed situations where the oxygen level was supersaturated (especially on May- 23, 25, 28, 29, 30 and June - 7 and 8) (Fig. 9a), and the DO level reached more than 8 mg/L. A total KE of 11.5 J/m^3 appears to be the threshold factor for this supersaturation (Fig. 9b), which could destroy the stratification and interrupt hypoxia formation in the nearshore waters. Concerning the increase of KE, the PE of the system is slightly reduced. The PE ranged between 9.9 to 10.08 J/m^3 with an average value of 10.03 J/m^3 . Although the variation of PE is negligible, during each upwelling (downwelling) event, the PE increases (decreases) slightly. The average tide and wind-induced KE was 2.02 and 4.18 J/m^3 , which means KE from local wind is two times higher than tide-induced KE. The maximum KE induced by tide and wind was 10.64 J/m^3 (during spring tide only) and 65.9 J/m^3 , respectively, with a maximum total KE of 66.87 J/m^3 . Compared to wind-induced KE, tidal KE alone cannot produce a supersaturation threshold for mixing the water column. However, the total KE (sum of wind and tide) higher than the threshold increases the DO level to supersaturation. KE induced by wind is the major reason for the increase in the DO level up to 8 mg/L. The combination of freshwater content (> 0.09) and wind-induced KE ($> 20 \text{ J/m}^3$) can further increase the DO up to 10 mg/L (25th and 28th May). According to the FF classification of Seena et al. (2019), a FF value between 0 and 0.15 is termed an estuarine plume-influenced region. An FF in the range 0 - 0.15 (Fig. 9e) indicated the mud bank region as freshwater-influenced by rainfall and river discharge. During each heavy rain event, the Irrigation Department of Thottappally spillway near the mud bank region (which effectively controls the Kuttanad region's flood level) has opened 35 shutters to ensure the smooth flow of floodwaters from Kuttanad into the Arabian Sea (Kamranuddin et al., 2021; Modi et al., 2021; Sreejith, 2013). The combination of wind and freshwater is the decisive factor determining the aeration of the water column up to supersaturation from 12:00 to 24:00 hours. There is always a time shift between offshore wind (upwelling from 00:00 to 12:00 hours) and local wind speed (wind-induced KE from 12:00 to 24:00 hours), as evident from Fig. 9b and c. The DO remains at its saturation levels when the upwelling ($ET > 1 \text{ m}^3/\text{sec}/\text{m}$) balances the KE ($> 11.5 \text{ J/m}^3$) generated by the wind-induced mixing (e.g. May- 24, 27 and 31). In the case of hypoxic conditions, the ET showed relatively high intensities of upwelling ($> 1 \text{ m}^3/\text{sec}/\text{m}$) from 00:00 to 12:00 hours, which can reduce the DO levels below 2 mg/L (e.g. 26th May and 6th June) with the absence of local wind (i.e. offshore wind for upwelling is more dominant than the local nearshore wind). DO levels depend on the dominance and subjugation of each factor, especially local wind speed/direction, upwelling/ET and FF. The KE of 11.5 J/m^3 equals a wind

speed of 5 m/s; persistence of wind speed > 5 m/s for more than 2 hours is sufficient for supersaturation. Even though the wind-induced KE exceeds the threshold for supersaturation, a strong upwelling event can balance the DO level at saturation (6.52 mg/L) or even be hypoxic when there is no local wind to mix the water column.

The study by Chen et al. (2015) in the Yangtze Estuary showed that a 10 % increase (decrease) in wind speed could decrease (increase) the extent of hypoxia to 46.66 % (67.28 %). The wind force is crucial in breaking stratification and ventilating bottom water, resulting in increased mixing (Goodrich et al., 1987). Lu et al. (2018) analysed the interactive role of wind stress and river discharge towards hypoxia. They concluded that hypoxia development involved river inputs of buoyancy and nutrients with weak wind stress, while hypoxia was inhibited when the wind stress was twice the mean wind stress. A system is prone to hypoxia if it has little physical energy (local wind force) and a high buoyancy input (precipitation/river discharge), which are its essential characteristics (Diaz, 2001). These observations indicate that wind can significantly influence the DO concentrations in the coastal environment even during a persistent upwelling period. Overall, the mixing of coastal water depends on the transformation between KE and PE induced by the combination of physical factors (Simpson, 1981; Simpson et al., 1990; Wang et al., 2022). Upwelling in the bottom waters and the freshwater content in the surface waters will create a strong stratification. The PE of the system increases during the upwelling process due to the vertical movement of water (Ferrari and Wunsch, 2009). Strong local wind force disrupts this stratification by converting the PE to KE by the movement and mixing of fluid particles. The KE is dissipated through viscosity into internal energy and converted to PE through buoyancy (Wunsch et al., 2004).

We also attempted to calculate the BVF of the buoy location water column based on the density at the buoy location and reference bottom density (1022 kg/m^3) from CTD. The study's findings show that during each upwelling event from 00:00 to 12:00 hours, there was a notable and consistent increase in the Brunt-Väisälä frequency (BVF). This increase in BVF is a strong indicator of enhanced stratification within the water column (Fig. 9d). Interestingly, under typical circumstances, the presence of freshwater might lead one to anticipate a subsequent increase in BVF from 12:00 to 24:00. However, the study's observations highlight a different scenario. During this period, the influence of local wind-induced mixing became evident. This wind-induced mixing resulted in a reduction in BVF, as is also clearly illustrated in Figure 9d. These observations indicate that while introducing freshwater could potentially promote stratification, the influence of local wind patterns and their mixing effects counteract this tendency. As a result, the water column experiences reduced stratification during the latter half of the day, as evidenced by the decrease in BVF. This interplay of processes has significant

implications for understanding the dynamics of the water column and the factors that influence it during upwelling events. However, it is crucial to acknowledge the uncertainty associated with these BVF calculations. The accuracy of density measurements, which forms the basis for BVF calculations, can introduce uncertainty due to the bottom density data's buoy location limitation. A drastic change in bottom density can significantly influence BVF and also give irregular results in BVF calculation. Even though the limitation persists, the bottom density variation along the transect showed negligible variation during May and July, which gives enough fidelity in the BVF calculation. The stability in bottom density supports the reliability of the data used for BVF assessment.

3.5 Biogeochemical implications

A schematic that summarises the factors influencing DO is shown in Fig. 10. During the southwest monsoon, a local wind speed below 5 m/s ($KE < 11.5 \text{ J/m}^3$) keeps the water column stratified. The high-saline coastal waters were overlaid by a warm, fresher, low-salinity lens restricting the sub-surface water from aeration, ultimately leading to nearshore hypoxia (Situation I). A wind speed well above 5 m/s ($KE > 11.5 \text{ J/m}^3$) can effectively break the water column stratification that can aerate the water column (generally observed after 12:00 hours in the Alappuzha mud bank) (Situation II). This suggests that the variation of DO in the mud bank region depends on the balance between upwelling and wind-induced mixing.

The cycles of hypoxic and normoxic waters within a day can significantly influence biogeochemical cycling and ecosystem functioning. The observation that hypoxic waters are intruding into the shallow coastal areas, including Alappuzha mud banks, has significant implications in explaining the uncertainties in the potential of mud banks as reasonable fishing grounds (Rao et al., 1984; Silas, 1984). The mud banks do not generally favour fish aggregation, but when there is stress, such as hypoxia, the fish tends to avoid hypoxic waters by migrating to the surface layers. It was a spectacular site to witness many people casting nets from the mud bank at knee depth and even handpicking prawns/sardines jumping out of the waters to the beaches, probably due to suffocation. Large shoals of sardine and other pelagic fishes were found to be washed ashore on the southwest coast of India, where the role of diurnal variations in DO is significant (Kripa et al., 2018).

Hypoxia can significantly alter redox conditions, leading to changes in nitrogen cycling, and such modifications can induce the formation of nitrous oxide, retention and release of phosphorus and trace elements (Naqvi et al., 2000; Neubacher et al., 2011). Iron regeneration is lowest under fully oxic and permanent anoxic conditions and highest under low oxygen or alternating oxic-anoxic conditions (Mathew et al., 2022). Animals can move away from hypoxic areas, but sessile organisms experience

physiological stress and perish depending on the intensity, frequency, and duration of hypoxic events (Levin et al., 2003; Middelburg and Levin, 2009).

4. Conclusion

The temperature, salinity and DO were measured at 30-minute intervals from April to July 2022 from a mud bank region in the southeastern Arabian Sea through moored sensors. The data revealed the incursion of low temperature and hypoxic waters in the nearshore region by the third week of May. Significant diurnal variations in the DO characterised the southwest monsoon. The daily cycles of hypoxia and normoxia were noticed during June-July, and the duration of hypoxia was found to be significantly increasing when the monsoon progressed. The nearshore waters exhibited significant diurnal variations of DO and reached hypoxic conditions by 6:00 hours, persisted from 6:00 to 12:00 hours and then increased to supersaturated levels. The wind was the major factor controlling the deoxygenation and oxygenation of the nearshore waters. During the first half of the day, the weak winds keep the water column stratified, leading to hypoxia. In contrast, the strong northerly wind after 12:00 hours breaks the water column stratification, leading to a supersaturated phase. The transformation between KE and PE induced by wind and upwelling regulates this DO level. A sharp nighttime increase of DO up to 10 mg/L is observed in this study from 12:00 to 24:00 hours. The statistical analysis also showed that local wind speed and FF (> 0.09) are the primary reasons for hypoxia interruption and supersaturation. A northerly local wind speed > 5 m/s (more than two hours) can disturb the stratification, modulate upwelling and enhance the mixing process from 12:00 to 24:00 hours. The total kinetic energy of 11.5 J/m³ is found to be a threshold for this supersaturation. Further studies are essential to understand the biogeochemical and ecological implications of alternating oxic-hypoxic conditions in nearshore waters.

Authorship contribution statement

Abdul Azeez, S: Formal analysis, Investigation, Visualization, Writing-Original Draft. Gireeshkumar T R: Data curation, Investigation, Validation, Writing, Review and Editing, Funding Acquisition. Vignesh, E.R.: Sampling, Formal Analysis. Muraleedharan K R: Funding Acquisition, Project Administration, Review and Editing. Jaleel, A. K.U: Sampling, Investigation, Review and Editing. Arya, K.S: Sampling, Formal Analysis, Validation. Ravikumar Nair, C: Formal Analysis. Ratheesh, R: Review and Editing, Funding Acquisition.

Data availability

Data is submitted to the data centre of the CSIR-National Institute of Oceanography, and the data can be made available as per the terms and conditions of the institute.

Declaration of competing interest

The authors declare that they have no known competing financial interests or personal relationships that could have appeared to influence the work reported in this paper.

Ethical approval

This article does not contain any studies with human participants or animals performed by any authors.

Acknowledgements

The authors thank the facilities and support the Director, CSIR-National Institute of Oceanography, and the Scientist in Charge, Regional Centre-Kochi provided. We appreciate the services rendered by our colleagues at CSIR-NIO in successfully carrying out the field sampling and mooring. We thank the Ministry of Earth Sciences, Government of India, for financial support (Grant No. MoES/36/OOIS/Extra/22/2016). We thank Prof. A. N. Balchand for The critical comments given by the anonymous reviewers have considerably helped to improve the clarity of the manuscript.

References

- Altieri, A.H., Harrison, S.B., Seemann, J., Collin, R., Diaz, R.J., Knowlton, N., 2017. Tropical dead zones and mass mortalities on coral reefs. *Proc. Natl. Acad. Sci.* 114, 3660–3665.
- Aristizábal, M.F., Fewings, M.R., Washburn, L., 2016. Contrasting spatial patterns in the diurnal and semidiurnal temperature variability in the Santa Barbara Channel, California. *J. Geophys. Res. Ocean.* 121, 427–440.
- Army, U.S., n.d. Coastal Engineering Research Center, 1977. Shore Protection Manual. US Army, Corps Eng. Coast. Eng. Res. Center, Fort Belvoir, VA.
- Azeez, A., Revichandran, C., John, S., Seena, G., Nair, R.C., others, 2021. Sound speed variation in the coastal waters off Cochin and signature of subsurface maxima. *Ocean Dyn.* 71, 923–933.
- Balachandran, K.K., 2004. Does subterranean flow initiate mud banks off the southwest coast of India? *Estuar. Coast. Shelf Sci.* 59, 589–598.
- Banse, K., 1959. On upwelling and bottom-trawling off the southwest coast of India. *J. Mar. Biol. Assoc. India* 1, 33–49.
- Bonicelli, J., Moffat, C., Navarrete, S.A., Largier, J.L., Tapia, F.J., 2014. Spatial differences in thermal structure and variability within a small bay: interplay of diurnal winds and tides. *Cont. Shelf Res.* 88, 72–80.

- Booth, J.A.T., McPhee-Shaw, E.E., Chua, P., Kingsley, E., Denny, M., Phillips, R., Bograd, S.J., Zeidberg, L.D., Gilly, W.F., 2012. Natural intrusions of hypoxic, low pH water into nearshore marine environments on the California coast. *Cont. Shelf Res.* 45, 108–115.
- Breitburg, D., 2002. Effects of hypoxia, and the balance between hypoxia and enrichment, on coastal fishes and fisheries. *Estuaries* 25, 767–781.
- Chacko, K. V, Kumar, P.V.H., Kumar, M.R.R., Mathew, B., Bannur, V.M., 2012. A note on arabian sea warm Pool and its possible relation with monsoon onset over Kerala. *Int. J. Sci. Res. Publ.* 2, 1–4.
- Chen, X., Shen, Z., Li, Y., Yang, Y., 2015. Physical controls of hypoxia in waters adjacent to the Yangtze Estuary: A numerical modeling study. *Mar. Pollut. Bull.* 97, 349–364.
- Cropper, T.E., Hanna, E., Bigg, G.R., 2014. Spatial and temporal seasonal trends in coastal upwelling off Northwest Africa, 1981--2012. *Deep Sea Res. Part I Oceanogr. Res. Pap.* 86, 94–111.
- Dean, R.G., Dalrymple, R.A., 1991. *Water wave mechanics for engineers and scientists.* world scientific publishing company.
- Diaz, R.J., 2001. Overview of hypoxia around the world. *J. Environ. Qual.* 30, 275–281.
- Diaz, R.J., Rosenberg, R., Rabalais, N.N., Levin, L.A., 2009. Dead zone dilemma. *Mar. Pollut. Bull.* 58, 1767–1768.
- Donis, D., Mantzouki, E., McGinnis, D.F., Vachon, D., Gallego, I., Grossart, H.-P., de Senerpont Domis, L.N., Teurlincx, S., Seelen, L., Lüring, M., others, 2021. Stratification strength and light climate explain variation in chlorophyll a at the continental scale in a European multilake survey in a heatwave summer. *Limnol. Oceanogr.* 66, 4314–4333.
- Fennel, K., Testa, J.M., 2019. Biogeochemical controls on coastal hypoxia. *Ann. Rev. Mar. Sci.* 11, 105–130.
- Ferrari, R., Wunsch, C., 2009. Ocean circulation kinetic energy: Reservoirs, sources, and sinks. *Annu. Rev. Fluid Mech.* 41, 253–282.
- Gireeshkumar, T.R., Mathew, D., Pratihary, A.K., Naik, H., Narvekar, K.U., Araujo, J., Balachandran, K.K., Muraleedharan, K.R., Thorat, B., Nair, M., others, 2017. Influence of upwelling induced near shore hypoxia on the Alappuzha mud banks, South West Coast of India. *Cont. Shelf Res.* 139, 1–8.
- Gireeshkumar, T.R., Mathew, D., Udayakrishnan, P.B., Shameem, K., KP, F.F., Furtado, C.M., Deepulal, P.M., Nair, M., Balachandran, K.K., 2020. Montmorillonite and phosphorus enrichment in sediments as the causative factor for mud bank formation along the southwest coast of India. *Reg. Stud. Mar. Sci.* 40, 101517.
- Goodrich, D.M., Boicourt, W.C., Hamilton, P., Pritchard, D.W., 1987. Wind-induced destratification in Chesapeake Bay. *J. Phys. Oceanogr.* 17, 2232–2240.

- Gopalakrishna, V. V., Durand, F., Nisha, K., Lengaigne, M., Boyer, T.P., Costa, J., Rao, R.R., Ravichandran, M., Amrithash, S., John, L., others, 2010. Observed intra-seasonal to interannual variability of the upper ocean thermal structure in the southeastern Arabian Sea during 2002--2008. *Deep Sea Res. Part I Oceanogr. Res. Pap.* 57, 739–754.
- Gopinathan, C.K., Qasim, S.Z., 1974. Mud banks of Kerala-their formation and characteristics. *Indian J. Mar. Sci.* 3, 105–114.
- Grantham, B.A., Chan, F., Nielsen, K.J., Fox, D.S., Barth, J.A., Huyer, A., Lubchenco, J., Menge, B.A., 2004. Upwelling-driven nearshore hypoxia signals ecosystem and oceanographic changes in the northeast Pacific. *Nature* 429, 749–754.
- Gupta, G.V.M., Sudheesh, V., Sudharma, K. V, Saravanane, N., Dhanya, V., Dhanya, K.R., Lakshmi, G., Sudhakar, M., Naqvi, S.W.A., 2016. Evolution to decay of upwelling and associated biogeochemistry over the southeastern Arabian Sea shelf. *J. Geophys. Res. Biogeosciences* 121, 159–175.
- Huang, J., Hu, J., Li, S., Wang, B., Xu, Y., Liang, B., Liu, D., 2019. Effects of physical forcing on summertime hypoxia and oxygen dynamics in the Pearl River Estuary. *Water* 11, 2080.
- Jayaram, C., Kumar, P.K.D., 2018. Spatio-temporal variability of upwelling along the southwest coast of India based on satellite observations. *Cont. Shelf Res.* 156, 33–42.
- Johannessen, O.M., Subbaraju, G., Blindheim, J., 1987. Seasonal variations of the oceanographic conditions off the southwest coast of India during 1971-1975.
- Jyothibabu, R., Balachandran, K.K., Jagadeesan, L., Karnan, C., Arunpandi, N., Naqvi, S.W.A., Pandiyarajan, R.S., 2018. Mud Banks along the southwest coast of India are not too muddy for plankton. *Sci. Rep.* 8, 2544.
- Kamranuddin, K., Reddy, C.H.S., Prathap, J.R., 2021. Flood Mitigation and River Pamba in Kerala-- Insights and Measures with Special Reference to Thottappally.
- Kaplan, D.M., Largier, J.L., Navarrete, S., Guíñez, R., Castilla, J.C., 2003. Large diurnal temperature fluctuations in the nearshore water column. *Estuar. Coast. Shelf Sci.* 57, 385–398.
- Karnan, C., Jyothibabu, R., Arunpandi, N., Jagadeesan, L., Muraleedharan, K.R., Pratihari, A.K., Balachandran, K.K., Naqvi, S.W.A., 2017. Discriminating the biophysical impacts of coastal upwelling and mud banks along the southwest coast of India. *J. Mar. Syst.* 172, 24–42.
- Kokoszka, F., Le Roux, B., Iudicone, D., Conversano, F., Ribera d'Alcalá, M., 2023. Long-term variability of the coastal ocean stratification in the Gulf of Naples: Two decades of monitoring the marine ecosystem at the LTER--MC site, between land and open Mediterranean Sea. *Mar. Ecol.* 44, e12725.
- Kripa, V., Mohamed, K.S., Koya, K.P.S., Jeyabaskaran, R., Prema, D., Padua, S., Kuriakose, S., Anilkumar, P.S., Nair, P.G., Ambrose, T. V, others, 2018. Overfishing and climate drives changes in biology and recruitment of the Indian oil sardine *Sardinella longiceps* in southeastern Arabian Sea. *Front. Mar. Sci.* 5, 443.

- Kumar, P.V.H., Anand, P., 2016. Coastal upwelling off the southwest coast of India : observations and simulations Coastal upwelling off the southwest coast of India: observations 8947. <https://doi.org/10.1080/17538947.2016.1216614>
- Levin, L.A., Rathburn, A.E., Gutiérrez, D., Muñoz, P., Shankle, A., 2003. Bioturbation by symbiont-bearing annelids in near-anoxic sediments: implications for biofacies models and paleo-oxygen assessments. *Palaeogeogr. Palaeoclimatol. Palaeoecol.* 199, 129–140.
- Liu, G., He, W., Cai, S., 2020. Seasonal variation of dissolved oxygen in the Southeast of the Pearl River Estuary. *Water* 12, 2475.
- Lu, Z., Gan, J., Dai, M., Liu, H., Zhao, X., 2018. Joint effects of extrinsic biophysical fluxes and intrinsic hydrodynamics on the formation of hypoxia west off the Pearl River Estuary. *J. Geophys. Res. Ocean.* 123, 6241–6259.
- Mac Pherson, H., Kurup, P.G., 1981. Wave damping at the Kerala mudbanks.
- Mathew, B., KUMAR, P.V.H., Rao, R.R., 2003. Mixed layer variability at selected locations in the Arabian Sea during pre and summer monsoon seasons: Observations and simulations. *Mausam* 54, 917–928.
- Mathew, D., Gireeshkumar, T.R., Balachandran, K.K., Udayakrishnan, P.B., Shameem, K., Deepulal, P.M., Nair, M., Madhu, N. V, Muraleedharan, K.R., 2020. Influence of hypoxia on phosphorus cycling in Alappuzha mud banks, southwest coast of India. *Reg. Stud. Mar. Sci.* 34, 101083.
- Mathew, D., Gireeshkumar, T.R., Udayakrishnan, P.B., Shameem, K., Nayana, P.M., Deepulal, P.M., Sarath, R., Nair, M., Jaleel, A.K.U., Balachandran, K.K., 2022. Geochemical speciation of iron under nearshore hypoxia: A case study of Alappuzha mud banks, southwest coast of India. *Cont. Shelf Res.* 238, 104686.
- Mathew, J., Baba, M., 1995. Mudbanks of the southwest coast of India. II: Wave-mud interactions. *J. Coast. Res.* 179–187.
- Middelburg, J.J., Levin, L.A., 2009. Coastal hypoxia and sediment biogeochemistry. *Biogeosciences* 6, 1273–1293.
- Modi, A., Nair, T.M., Remya, P.G., Harikumar, R., Srinivas, K., Srinivas, G., 2021. The role of anomalous oceanic features on enhancing flooding duration in Kuttanad region, Kerala (India). *J. Earth Syst. Sci.* 130, 1–10.
- Muraleedharan, K.R., Kumar, P.K.D., Kumar, S.P., John, S., Srijith, B., Kumar, K.A., Kumar, K.N., Gautham, S., Samiksha, V., 2018. Formation mechanism of mud bank along the Southwest Coast of India. *Estuaries and coasts* 41, 1021–1035.
- Muraleedharan, K.R., Kumar, P.K.D., Kumar, S.P., Srijith, B., John, S., Kumar, K.R.N., 2017. Observed salinity changes in the Alappuzha mud bank, southwest coast of India and its implication to hypothesis of mudbank formation. *Cont. Shelf Res.* 137, 39–45.
- Naqvi, S., Naik, H., Jayakumar, D.A., Shailaja, M.S., Narvekar, P. V, 2006. Seasonal oxygen deficiency over the western continental shelf of India, in: *Past and Present Water Column Anoxia*. Springer, pp. 195–224.

- Naqvi, S.W.A., Jayakumar, D.A., Narvekar, P. V, Naik, H., Sarma, V., D'souza, W., Joseph, S., George, M.D., 2000. Increased marine production of N₂O due to intensifying anoxia on the Indian continental shelf. *Nature* 408, 346.
- Narvekar, J., Roy Chowdhury, R., Gaonkar, D., Kumar, P.K.D., Prasanna Kumar, S., 2021. Observational evidence of stratification control of upwelling and pelagic fishery in the eastern Arabian Sea. *Sci. Rep.* 11, 7293.
- Neubacher, E.C., Parker, R.E., Trimmer, M., 2011. Short-term hypoxia alters the balance of the nitrogen cycle in coastal sediments. *Limnol. Oceanogr.* 56, 651–665.
- Philip, A.S., Babu, C.A., Hareeshkumar, P. V, 2013. Meteorological aspects of mud bank formation along south west coast of India. *Cont. Shelf Res.* 65, 45–51.
- Rao, A.D., Joshi, M., Ravichandran, M., 2008. Oceanic upwelling and downwelling processes in waters off the west coast of India. *Ocean Dyn.* 58, 213–226.
- Rao, D.S., Mathew, K.J., Gopinathan, C.P., Regunathan, A., Murty, A.V.S., 1984. Ecology of mudbanks-Hydrography. *C. Bull.* 31, 25–27.
- Rao, R.R., Kumar, M.S.G., Ravichandran, M., Rao, A.R., Gopalakrishna, V. V, Thadathil, P., 2010. Interannual variability of Kelvin wave propagation in the wave guides of the equatorial Indian Ocean, the coastal Bay of Bengal and the southeastern Arabian Sea during 1993--2006. *Deep Sea Res. Part I Oceanogr. Res. Pap.* 57, 1–13.
- Ray, S., Swain, D., Ali, M.M., Bourassa, M.A., 2022. Coastal Upwelling in the Western Bay of Bengal: Role of Local and Remote Windstress. *Remote Sens.* 14, 4703.
- Reid, R.O., 1957. Modification of the quadratic bottom-stress law for turbulent channel flow in the presence of surface wind-stress. *US Beach Erosion Board.*
- Samiksha, S. V, Vethamony, P., Rogers, W.E., Pednekar, P.S., Babu, M.T., Dineshkumar, P.K., 2017. Wave energy dissipation due to mudbanks formed off southwest coast of India. *Estuar. Coast. Shelf Sci.* 196, 387–398.
- Seena, G., Muraleedharan, K.R., Revichandran, C., Azeez, S.A., John, S., 2019. Seasonal spreading and transport of buoyant plumes in the shelf off Kochi, South west coast of India-A modeling approach. *Sci. Rep.* 9, 1–15.
- Seena, G., Muraleedharan, K.R., Revichandran, C., Azeez, S.A., John, S., Nair, R.C., 2022. Time-dependent plume front positioning and its dynamics coupled with seasonal river efflux. *Ocean Dyn.* 72, 207–222.
- Seshappa, G., 1953. Phosphate content of mudbanks along the Malabar coast. *Nature* 171, 526–527.
- Seshappa, G., Jayaraman, R., 1956. Observations on the composition of bottom muds in relation to the phosphate cycle in the inshore waters of the Malabar Coast, in: *Proceedings of the Indian Academy of Sciences-Section B.* pp. 288–301.
- Shah, P., Sajeev, R., Gopika, N., 2015. Study of upwelling along the west coast of India A climatological approach. *J. Coast. Res.* 31, 1151–1158.

- Shah, P., Sajeev, R., Santhosh, K.M., Thara, K.J., Muhammad, S., John, K.L., George, G., 2018. Observed signals of upwelling and downwelling along the west coast of India. *Indian J. Geo-Marine Sci.* 47, 604–612.
- Shah, P., Sajeev, R., Thara, K.J., George, G., Shafeeque, M., Akash, S., Platt, T., 2019. A Holistic Approach to Upwelling and Downwelling along the South-West Coast of India. *Mar. Geod.* 42, 64–84.
- Shankar, D., Shetye, S.R., 1997. On the dynamics of the Lakshadweep high and low in the southeastern Arabian Sea. *J. Geophys. Res. Ocean.* 102, 12551–12562.
- Sharma, G.S., 1978. Upwelling off the southwest coast of India. *Indian J. Mar. Sci.* 7, 209–218.
- Shetye, S.R., 1984. Seasonal variability of the temperature field off the south-west coast of India. *Proc. Indian Acad. Sci. Planet. Sci.* 93, 399–411.
- Shetye, S.R., Gouveia, A.D., Shenoi, S.S.C., Sundar, D., Michael, G.S., Almeida, A.M., Santanam, K., 1990. Hydrography and circulation off the west coast of India during the southwest monsoon 1987. *J. Mar. Res.* 48, 359–378.
- Silas, E.G., 1984. Mudbanks of Kerala-Karnataka; need for integrated study. *C. Bull.* 31, 2–7.
- Simpson, J.H., 1981. The shelf-sea fronts: implications of their existence and behaviour. *Philos. Trans. R. Soc. London. Ser. A, Math. Phys. Sci.* 302, 531–546.
- Simpson, J.H., Brown, J., Matthews, J., Allen, G., 1990. Tidal straining, density currents, and stirring in the control of estuarine stratification. *Estuaries* 13, 125–132.
- Smitha, A., Joseph, K.A., Jayaram, C., Balchand, A.N., 2014. Upwelling in the southeastern Arabian Sea as evidenced by Ekman mass transport using wind observations from OCEANSAT--II Scatterometer.
- Smitha, B.R., Sanjeevan, V.N., Vimalkumar, K.G., Revichandran, C., 2008. On the upwelling off the southern tip and along the west coast of India. *J. Coast. Res.* 24, 95–102.
- Sreejith, K.A., 2013. Human impact on Kuttanad wetland ecosystem-An overview. *Int. J. Sci. Environ. Technol.* 2, 679–690.
- Sripoonpan, P., Saramul, S., 2021. Coastal upwelling investigation in the Gulf of Thailand using Ekman transport and sea surface temperature upwelling indices. *Eng. J.* 25, 1–16.
- Suneela, S.S., Sureshkumar, S., 2021. Characteristics of Mudbanks along the Southwest Coast of India. *Eart Envi Scie Res Rev*, 4 1 12.
- Sylas, E.G., 1984. Mudbanks of Kerala-Karnataka need for an integrated study. *Mudbanks Kerala Coast, Cent. Mar. Fish. Res. Inst. Bull. No.* 31.
- Van Dorn, W.C., 1953. Wind stress on an artificial pond. *J. Mar. Res.* 12.
- Vaquer-Sunyer, R., Duarte, C.M., 2008. Thresholds of hypoxia for marine biodiversity. *Proc. Natl. Acad. Sci.* 105, 15452–15457.

- Varela, R., Álvarez, I., Santos, F., DeCastro, M., Gómez-Gesteira, M., 2015. Has upwelling strengthened along worldwide coasts over 1982-2010? *Sci. Rep.* 5, 1–15.
- Walter, R.K., Woodson, C.B., Leary, P.R., Monismith, S.G., 2014. Connecting wind-driven upwelling and offshore stratification to nearshore internal bores and oxygen variability. *J. Geophys. Res. Ocean.* 119, 3517–3534.
- Wang, K., Yao, J., Wang, J., Liu, H., Yin, K., 2022. Role of Winds in Interrupting the Formation of Coastal Hypoxia. *Front. Mar. Sci.* 9.
- Wei, X., Zhan, H., Ni, P., Cai, S., 2016. A model study of the effects of river discharges and winds on hypoxia in summer in the Pearl River Estuary. *Mar. Pollut. Bull.* 113, 414–427.
- Weiss, R.F., 1970. The solubility of nitrogen, oxygen and argon in water and seawater, in: *Deep Sea Research and Oceanographic Abstracts*. pp. 721–735.
- WES-HL, U.S., 1996. Users Guide to RMA2 Version 4.3. US Army Corps Eng. Exp. Stn. Hydraul. Lab. Vicksburg, USA.
- Woodson, C.B., Eerkes-Medrano, D.I., Flores-Morales, A., Foley, M.M., Henkel, S.K., Hession-Lewis, M., Jacinto, D., Needles, L., Nishizaki, M.T., O’Leary, J., others, 2007. Local diurnal upwelling driven by sea breezes in northern Monterey Bay. *Cont. Shelf Res.* 27, 2289–2302.
- Wu, J., 1969. Wind stress and surface roughness at air-sea interface. *J. Geophys. Res.* 74, 444–455.
- Wunsch, C., Ferrari, R., others, 2004. Vertical mixing, energy, and the general circulation of the oceans. *Annu. Rev. Fluid Mech.* 36, 281–314.

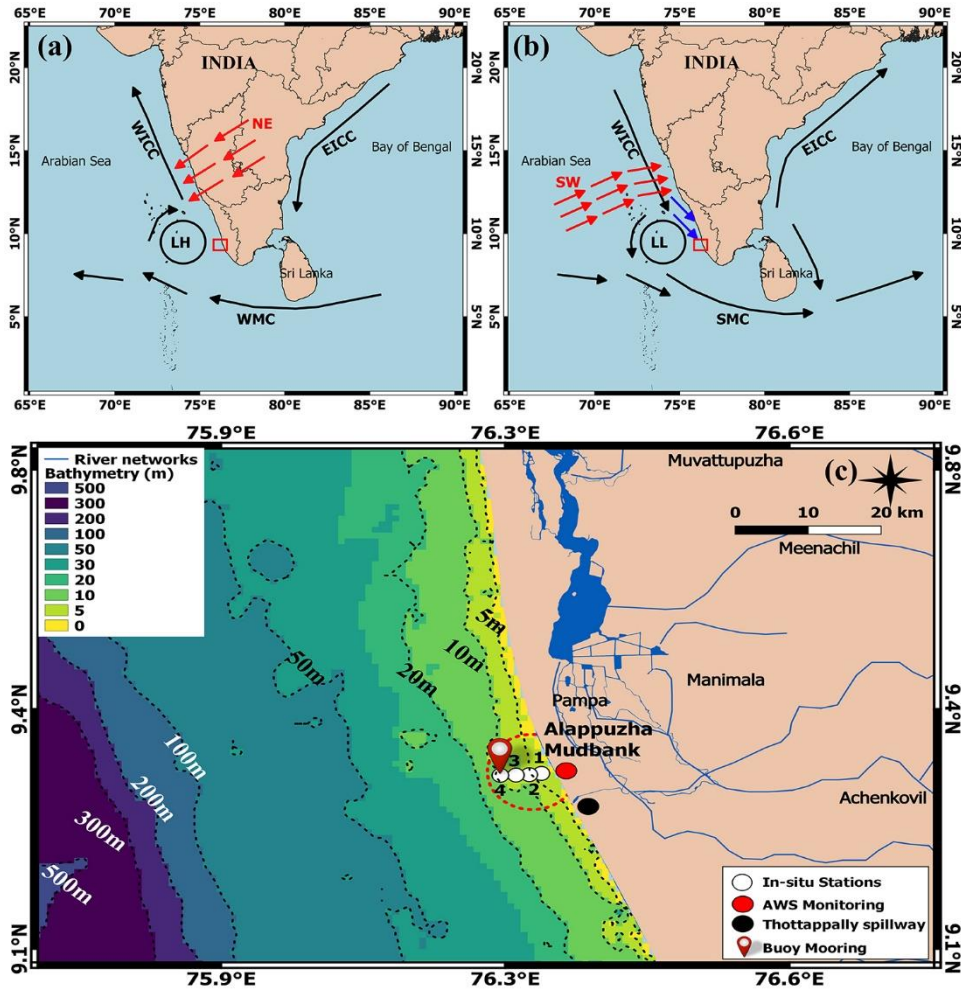


Figure 1. Schematic diagram representing the wind (red arrow) and current pattern (black arrow) during a) northeast and b) southwest monsoon along the Arabian Sea. The wind responsible for upwelling is shown in blue colour parallel to the coast. c) Map of the study region showing the locations of the cross-shelf stations (white dots, buoy mooring (autonomous observatory) and the AWS (black dot) installed on the shore. The abbreviations are WICC: West India Coastal Current, EICC: East India Coastal Current, WMC: Winter Monsoon Current, SMS: Summer Monsoon Current, LH: Lakshadweep High, LL: Lakshadweep low.

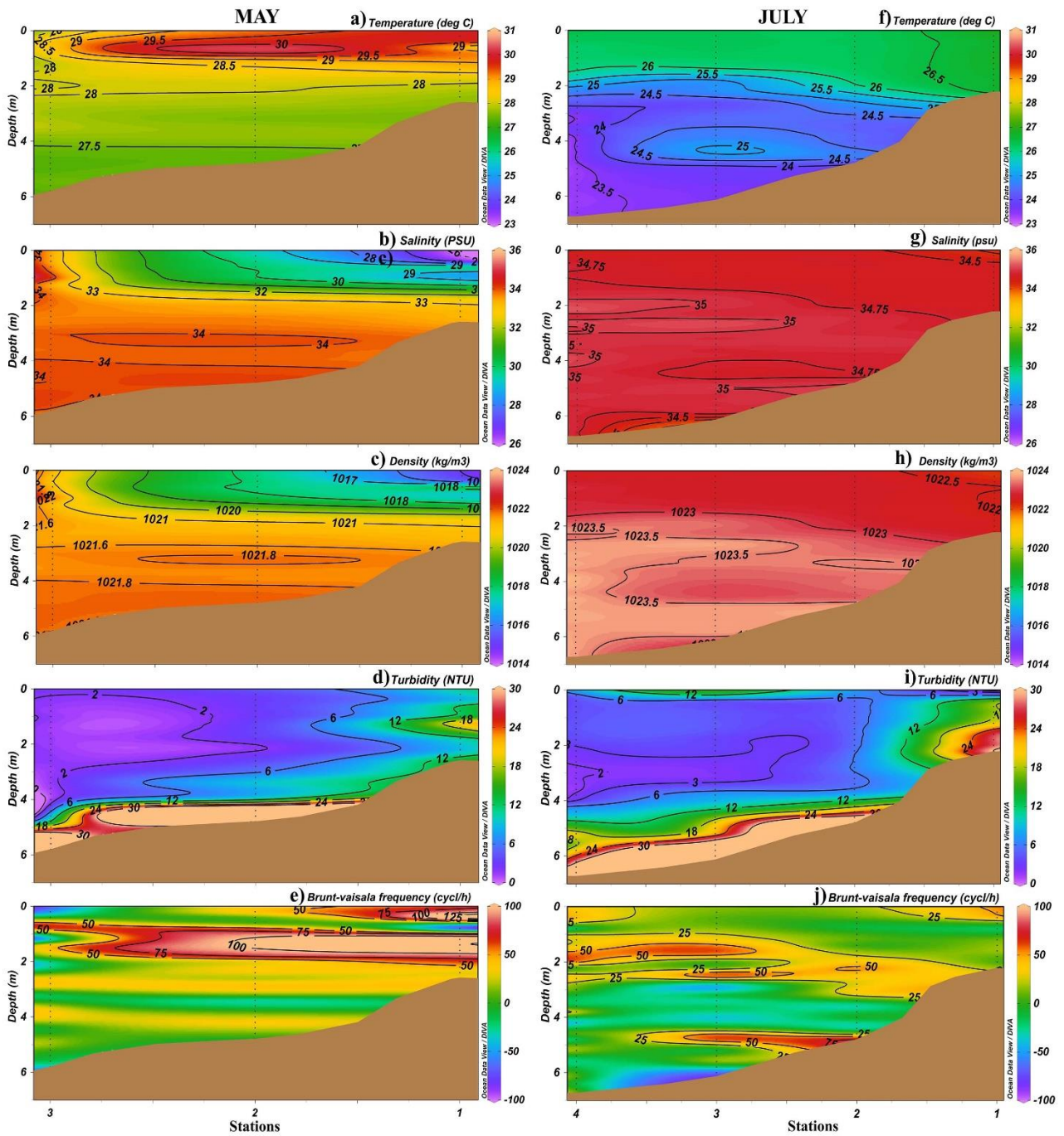


Figure 2. Cross-shelf variations of temperature, salinity, density, turbidity and Brunt-Vaisala frequency (derived parameter using equation 8) in the nearshore waters of Alappuzha during 22nd May 2022 between 10:14 to 12:24 hours (left panel from a to e) and 30th July 2022 between 08:30 to 10:24 hours (right panel from f to j).

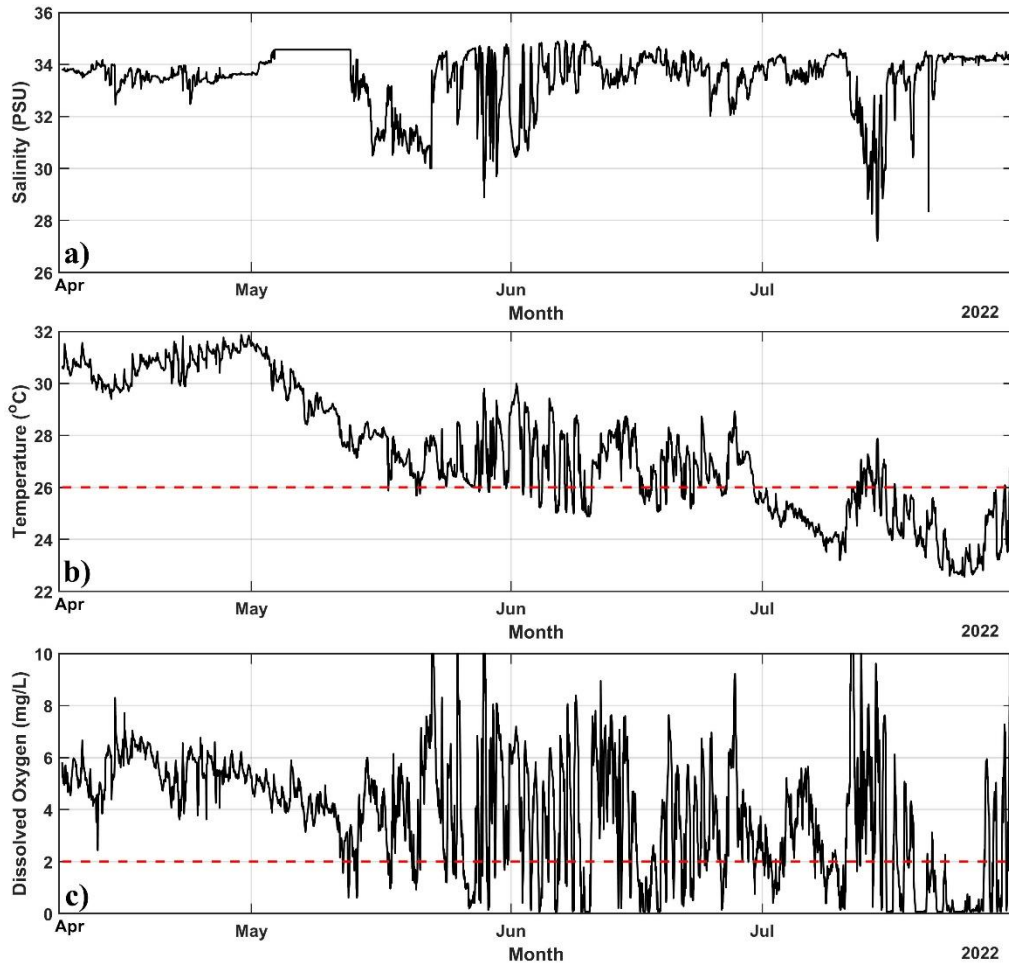


Figure 3. Hourly variations of a) salinity, b) temperature (dashed red line showed the 26 °C temperature index for upwelling) and c) dissolved oxygen (dashed red line showed the hypoxic condition less than 2mg/L) in the Alappuzha mud bank region at the buoy mooring location.

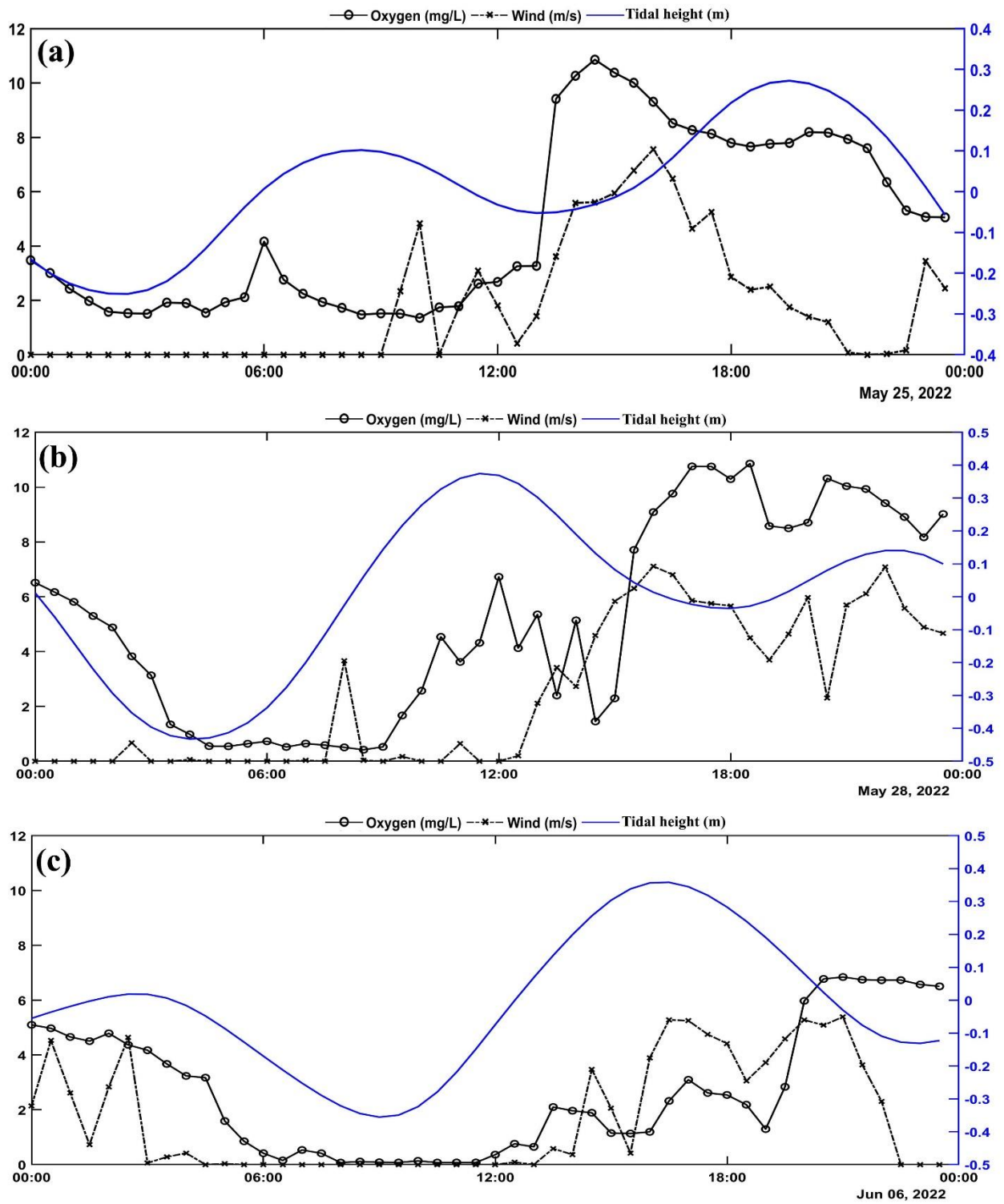


Figure 4. Diurnal variations of oxygen, wind speed and tide in the Alappuzha mud bank during a) 25th May 2022, b) 28th May 2022 and c) 6th June 2022.

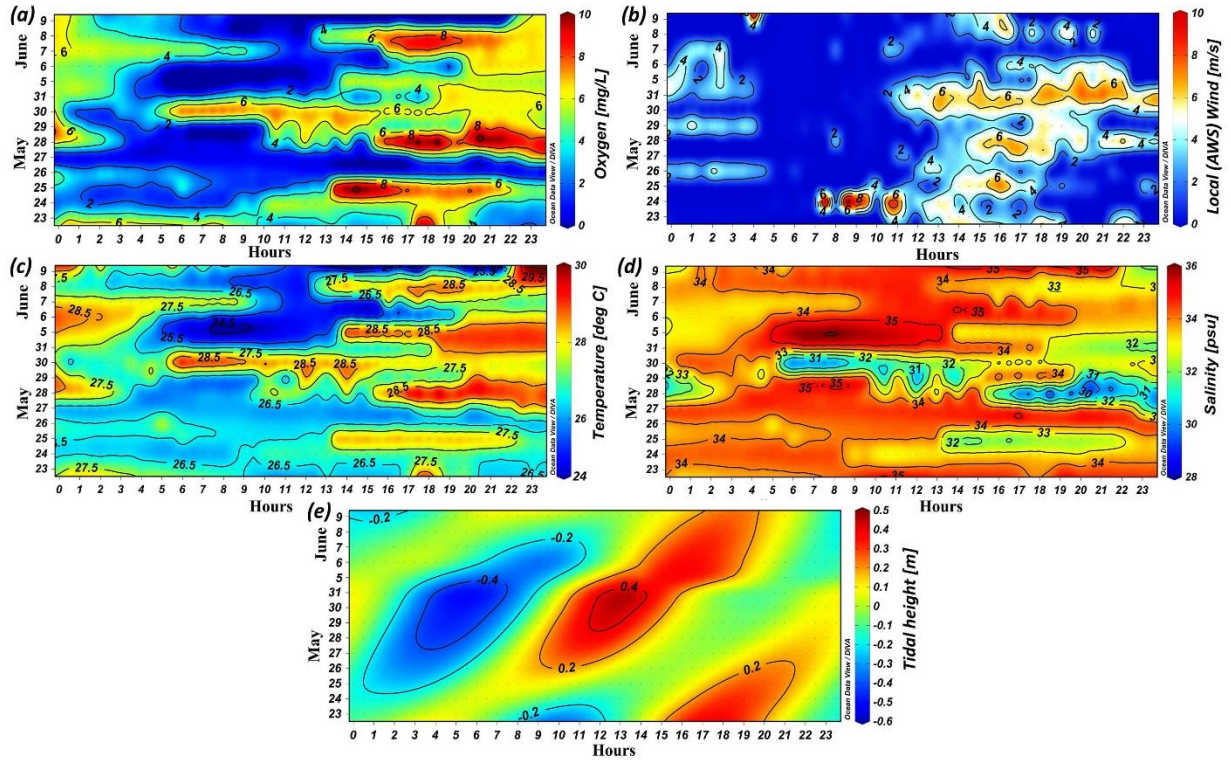


Figure 5. Hourly variation of a) oxygen, b) Local wind from AWS, c) temperature (colour shade) and salinity (contour lines), and d) tide from 23 May to 09 June 2022. There is no data between 1st to 4th of June 2022.

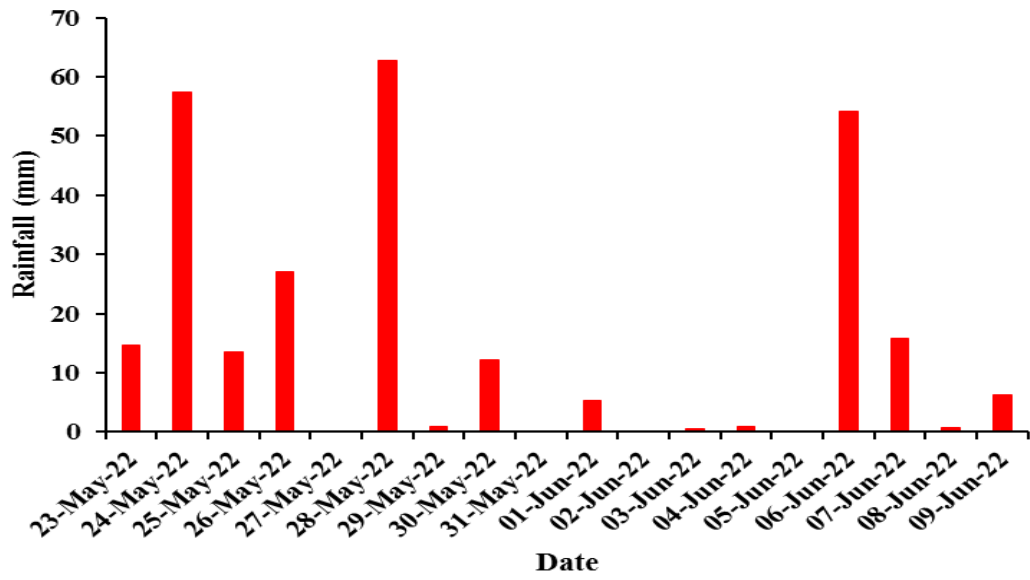


Figure 6. Daily rainfall data at the Ambalappuzha region from 23rd May 2022 to 9th June 2022.

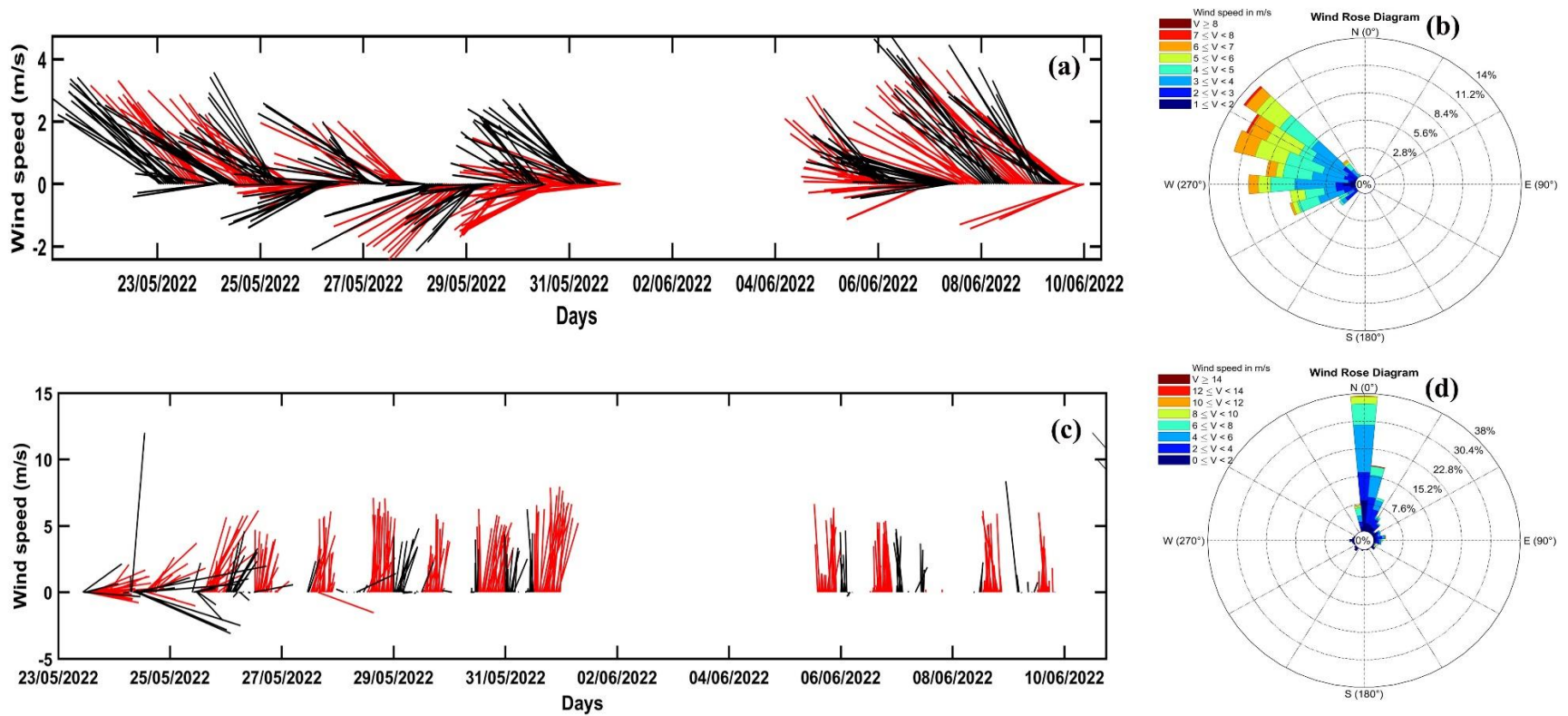


Figure 7. Stick plot and rose diagram of offshore wind (a & b) and local wind (c & d). Wind speed and direction indicated the south-westerly to north-westerly in the offshore region and mostly northerly in the nearshore region during the southwest monsoon. The local and offshore wind directions are favourable for upwelling.

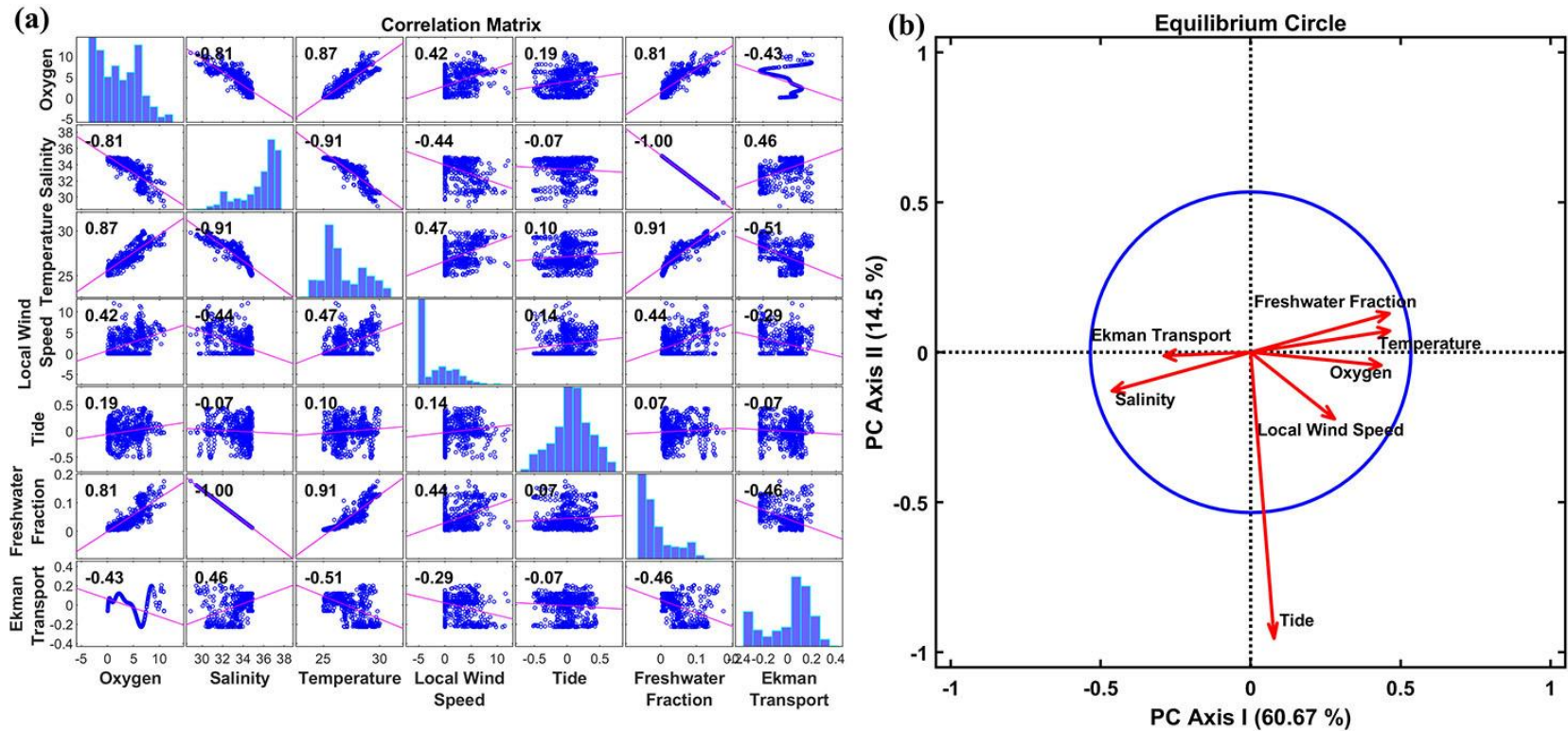


Figure 8. a) Correlogram analysis and b) PCA of oxygen, salinity, temperature, local wind speed, tide (height and currents), freshwater fraction and Ekman transport. The angular relationships between principal components on the factorial plane were used to assess the correlations between the variables. A small angle (close to 0°) indicated positive correlation, an angle of 90° suggested no correlation, and an angle of 180° signified negative correlation.

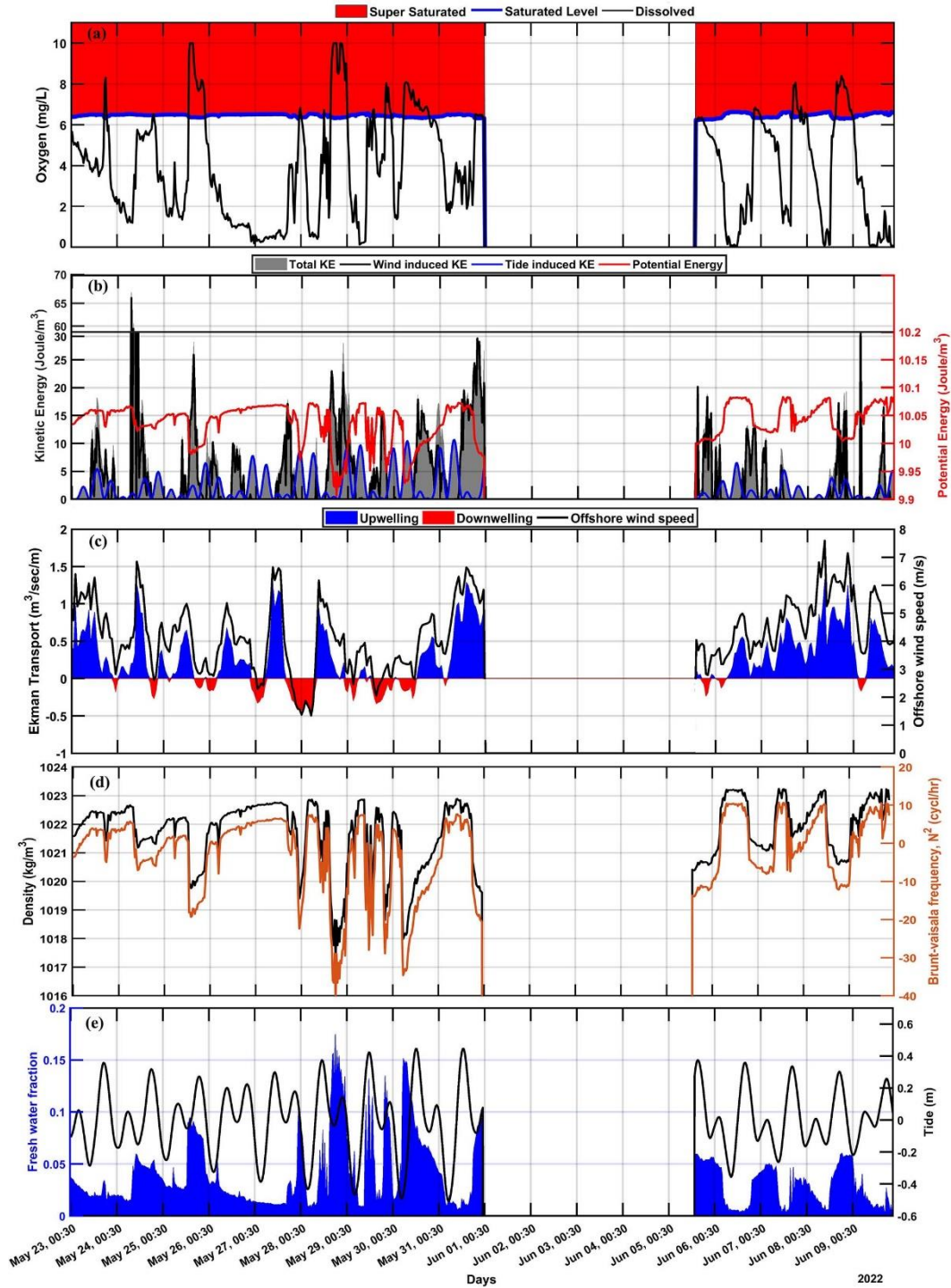


Figure 9. Variation of a) oxygen (dissolved, saturated and supersaturated), b) kinetic energy (wind-induced, tide-induced and total) and potential energy, c) Ekman Transport and offshore wind speed, d) Brunt-Vaisala Frequency and density e) freshwater fraction and tide from 23rd May 2022 to 9th June, 2022.

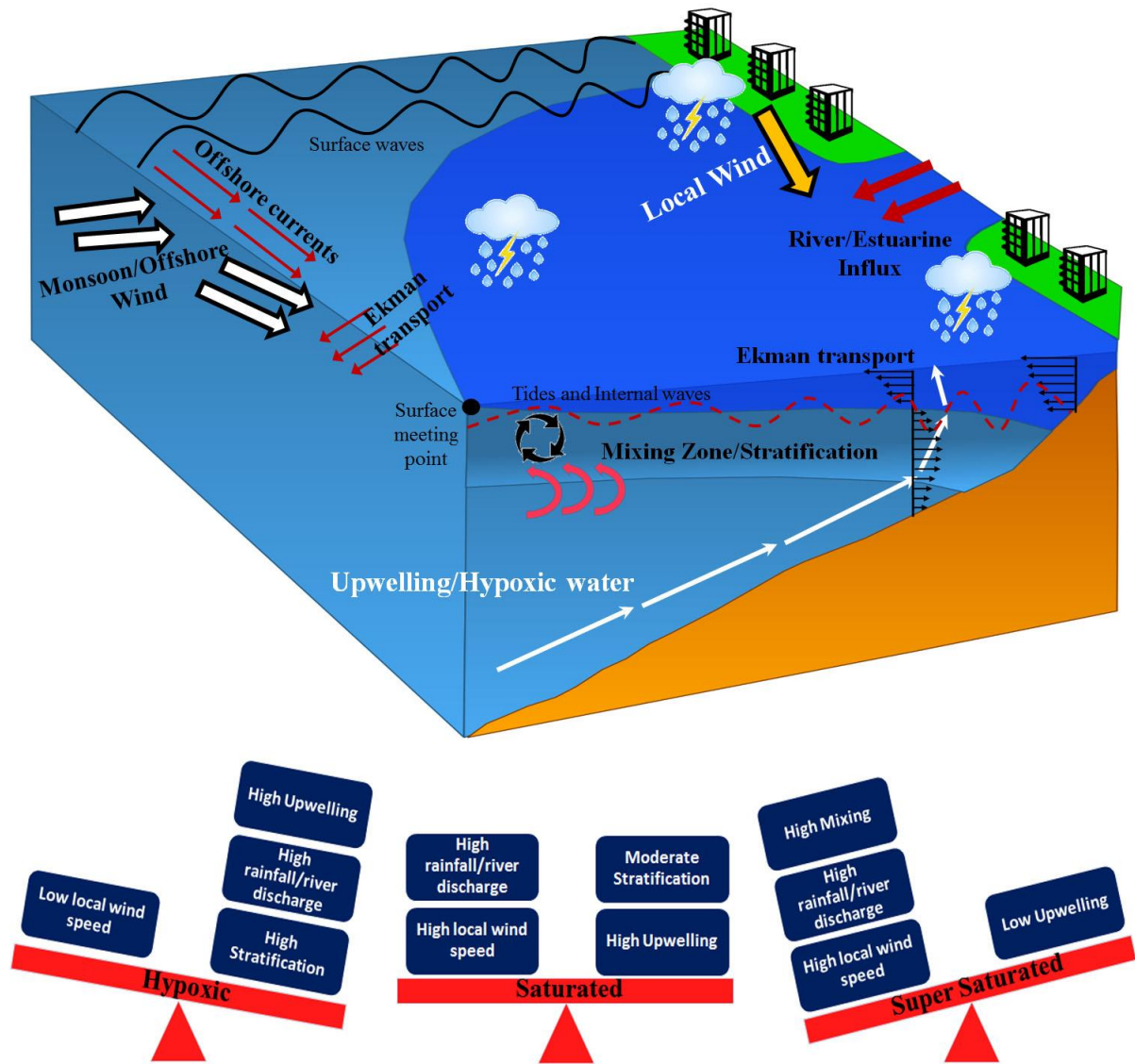


Figure 10. A schematic of the dynamics associated with the DO variation in the mud bank region.

Table 1 The average variation of the parameters Oxygen, Temperature, Salinity and Local wind speed from 00:00 AM to 12:00 hours and 12:00 to 24:00 hours

Parameter	00:00 to 12:00 hours	12:00 to 24:00 hours
Oxygen (mg/L)	2.96	6.7
Temperature (⁰ C)	26.4	27.5
Salinity (psu)	34.1	32.9
Local wind speed (m/s)	1.58	5